

IPCV: Information-Preserving Compression for MLLM Visual Encoders

Yuan Chen^{1,2*} Zichen Wen^{1,3*} Yuzhou Wu^{1,4} Xuyang Liu^{1,5} Shuang Chen¹
 Junpeng Ma⁶ Weijia Li^{7,3} Conghui He³ Linfeng Zhang^{1†}
¹ EPIC Lab, SJTU ² CityU ³ Shanghai AI Laboratory
⁴ University of Sheffield ⁵ SCU ⁶ FDU ⁷ SYSU

Abstract

*Multimodal Large Language Models (MLLMs) deliver strong vision-language performance but at high computational cost, driven by numerous visual tokens processed by the Vision Transformer (ViT) encoder. Existing token pruning strategies are inadequate: LLM-stage token pruning overlooks the ViT’s overhead, while conventional ViT token pruning, without language guidance, risks discarding textually critical visual cues and introduces feature distortions amplified by the ViT’s bidirectional attention. To meet these challenges, we propose IPCV, a training-free, information-preserving compression framework for MLLM visual encoders. IPCV enables aggressive token pruning inside the ViT via **Neighbor-Guided Reconstruction (NGR)** that temporarily reconstructs pruned tokens to participate in attention with minimal overhead, then fully restores them before passing to the LLM. Besides, we introduce **Attention Stabilization (AS)** to further alleviate the negative influence from token pruning by approximating the K/V of pruned tokens. It can be directly applied to previous LLM-side token pruning methods to enhance their performance. Extensive experiments show that IPCV substantially reduces end-to-end computation and outperforms state-of-the-art training-free token compression methods across diverse image and video benchmarks. Our code is available at <https://github.com/Perkzi/IPCV>.*

1. Introduction

Multimodal large language models (MLLMs) [25, 45] have achieved remarkable performance across diverse vision-language tasks [5, 15, 46, 47, 51, 57–59], benefiting from powerful language reasoning capabilities and strong vision encoders [39, 56]. However, the visual branch of these models often produces hundreds to thousands of tokens per image or video, especially at high resolutions or with

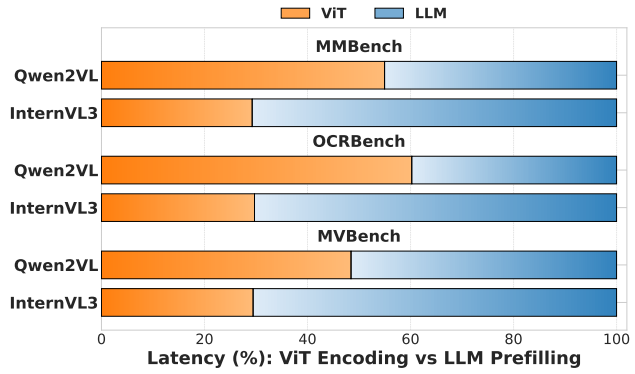


Figure 1. **ViT Encoding versus LLM Prefilling latency proportions** across three benchmarks—MMBench (low-resolution images), OCRBench (high-resolution images), and MVBench (videos)—using Qwen2-VL-7B-Instruct and InternVL3-38B.

multiple frames [6]. Due to the quadratic computational complexity $\mathcal{O}(N^2)$ of self-attention [44], longer token sequences incur significantly higher latency. This severely hinders the widespread adoption and edge deployment of MLLMs. In practice, however, visual tokens in MLLMs exhibit substantial redundancy [36]. To address this, a surge of recent research has focused on token pruning methods [26, 27, 29, 30, 50], which aim to directly reduce the number of tokens and lower computational costs.

Nevertheless, despite the remarkable progress of these approaches, most operate only on the LLM within MLLMs. In practice, as vision encoders increasingly adopt dynamic designs or higher native resolutions, the resulting visual token sequences grow significantly longer, rendering the computational cost of the vision encoder impossible to overlook (as shown in Figure 1). While several methods have been proposed for token compression at the vision transformer (e.g., ToMe [1], ToFu [16]), they primarily focus on vision-only models and tasks (e.g., classification), resulting in suboptimal performance on multimodal understanding tasks [60]. Generally speaking, token pruning in the ViT for MLLMs faces two significant challenges.

Absence of language guidance. A fundamental challenge

*Equal Contribution.

†Corresponding author: zhanglinfeng@sjtu.edu.cn

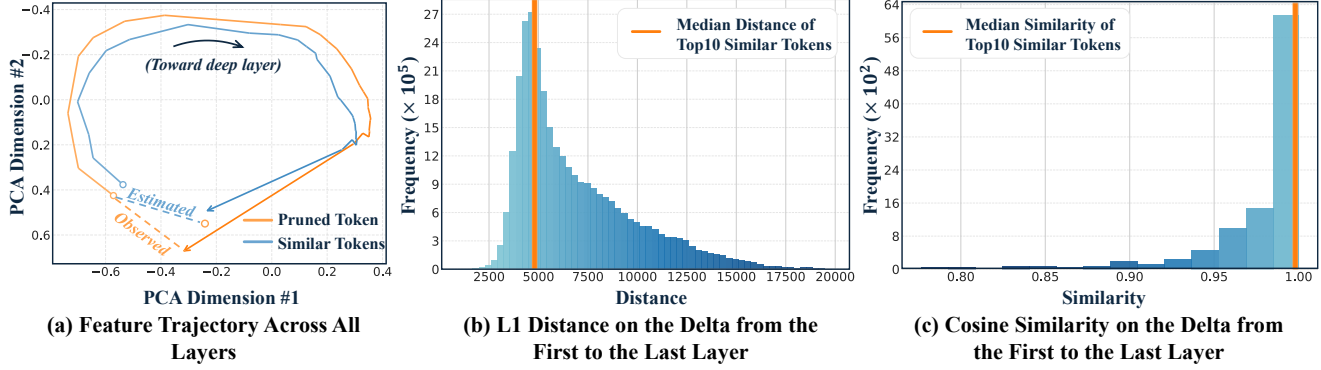


Figure 2. **Visualization of the delta of tokens from the shallow layers to the deep layers.** (a) PCA projection of the hidden state trajectories of a pruned token and the mean of its top-10 nearest neighbors, traced from the pruning layer to the final layer of the ViT, with arrows indicating the shift direction. (b) and (c): Distributions of L1 distance and cosine similarity, computed from pairwise comparisons between the change (delta) of retained tokens and that of pruned tokens across layers. The deep-blue vertical line denotes the overall median of the pairwise distances (cosine similarities) computed between each pruned token and the mean of its top-10 most similar tokens. These visualizations reveal that tokens with high similarity tend to exhibit highly similar changes from shallow to deep layers.

of performing token compression at the vision encoder in MLLMs lies in the absence of language guidance [48]. Since the token compression process occurs before any cross-modal interaction, it risks discarding visual tokens that may appear unimportant from a purely visual perspective but are in fact crucial for downstream language-driven reasoning.

Negative influence from pruned tokens. Moreover, the removal of certain vision tokens can introduce feature distortions in the remaining tokens, as the bidirectional attention mechanism in vision transformers [7] propagates information globally. This issue is even more pronounced at the vision encoding stage than in the language model, where unidirectional attention limits the scope of such errors [37, 41]. As a result, naive token pruning in the vision tower can inadvertently undermine the model’s ability to preserve information essential for multimodal understanding.

To tackle the above two challenges, we propose **Information-Preserving Compression** for MLLM Visual Encoders (**IPCV**). Specifically, in the vision encoder (i.e., ViT), IPCV prunes tokens in shallow layers to reduce the computation costs. Then, in the final layer, we introduce Neighbor-Guided Reconstruction (NGR), which aims to reconstruct the pruned tokens in the following layers based on their most similar remaining tokens (i.e., tokens that are not pruned). As studied in Figure 2, we find that similar tokens exhibit similar delta from the shallow layers to the deep layers. As a result, instead of directly copying the similar remaining tokens [1], NGR reconstructs the pruned tokens in the final layer by adding their values in the shallow layers with the delta of their most similar and remaining tokens from the shallow layers to the deep layers.

Secondly, to further reduce the negative influence of the pruned tokens on the remaining tokens, we introduce Attention Stabilization (AS), which aims to approximate the keys and values of pruned tokens in the middle layers, which is

achieved by reconstructing pruned tokens via NGR, and then computing their keys and values.

The proposed IPCV is training-free for the ViT and integrates seamlessly into diverse MLLMs. For the LLM stage, IPCV is orthogonal to and compatible with various token compression schemes; in this paper, we pair IPCV by default with the LLM-stage compressor in DART [49] to further reduce redundancy after modal fusion. In summary, our main contributions are as follows:

- We provide a systematic comparison of LLM-stage and ViT-stage token pruning in MLLMs, revealing the need and challenges for vision-side token pruning in MLLMs.
- We propose **IPCV**, a training-free vision-side token pruning framework that uses Neighbor-Guided Reconstruction (NGR) to deliver a semantically complete vision token set to the LLM, and Attention Stabilization (AS) to mitigate negative influence from pruned tokens.
- Extensive experiments on various benchmarks with two representative MLLM models demonstrate our effectiveness across diverse tasks and settings.

2. Related Work

Visual Compression in MLLM. To reduce the inflow of visual tokens into the LLM, recent work compresses at multiple junctures [12, 13, 23, 28, 34, 52]. At the projector, adaptive pooling (DeCo [54]) and query-based projectors (BLIP-2’s Q-Former [18]) shorten the sequence before it enters the language model. Within the LLM, methods include training-based policies guided by cross-modal supervision (e.g., LVPruning [43], Skip-Vision [55]) and training-free heuristics that use attention or feature similarity to prune or merge tokens dynamically during inference (e.g., FastV [3], SparseVLM [60], DART [49], EfficientVLA [53]). However, since a significant portion of computation already occurs in

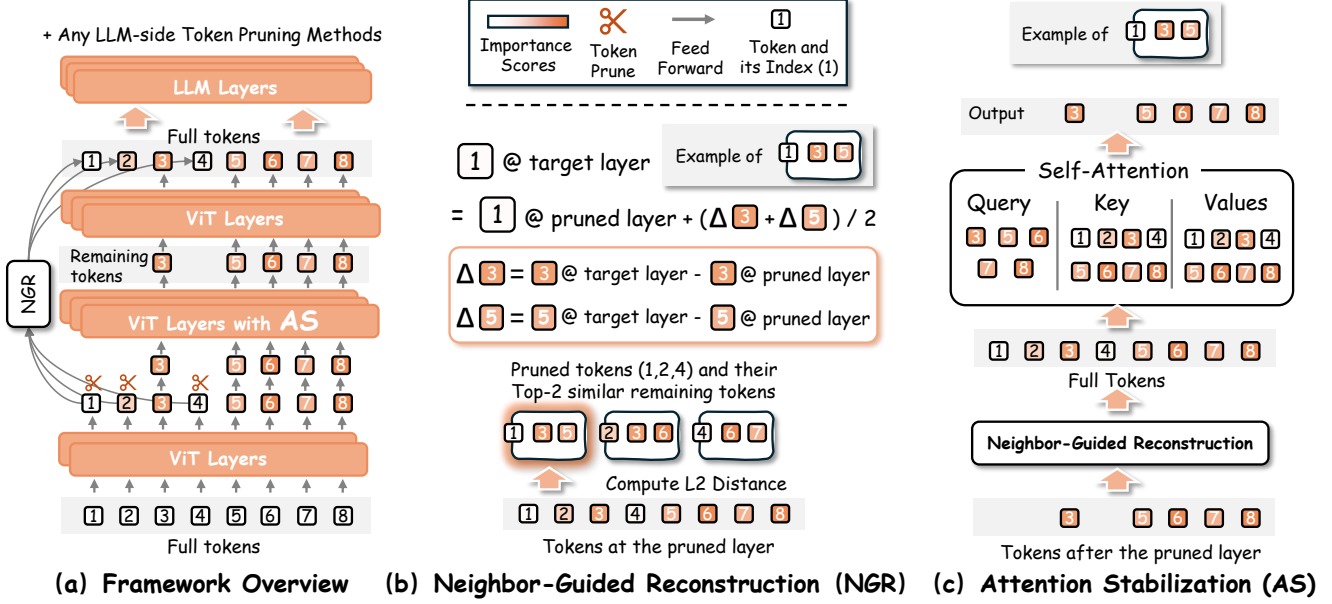


Figure 3. **Overview of IPCV.** IPCV prunes redundant visual tokens in the shallow layers of the vision encoder to reduce computation, then reconstructs the pruned tokens at the final layer using Neighbor-Guided Reconstruction (NGR) to deliver a semantically complete token set to the LLM. Attention Stabilization (AS) further mitigates the negative impact of token pruning by approximating the keys and values of the removed tokens in intermediate layers.

the ViT, where the initial visual tokens are processed, compression applied only within the LLM can provide only limited acceleration, as the vision encoder remains a bottleneck for overall efficiency.

Visual Compression in Visual Encoders. In visual encoders, token count can be reduced structurally or dynamically. Structurally, multi-scale encoders and hierarchical backbones with patch merging (e.g., LLaMA-VID [21], Swin Transformer [33]) progressively lower spatial or temporal resolution across stages, thus reducing the number of tokens. Dynamically, tokens are compressed within transformer layers: Token Merging (ToMe) [1] merges redundancy, while pruning within the ViT (DynamicViT [40], EViT [22], SparseViT [4]) removes low-importance tokens and reduces encoder computation. Most methods target single ViTs rather than MLLMs and often require extra training, which is costly in the MLLM setting.

3. Methodology

Token compression in the vision encoder of MLLMs inherently risks discarding tokens that appear visually redundant but are semantically important. IPCV is designed to solve this problem (see Figure 3): In the early ViT layers, redundant tokens are pruned to reduce computation. Their semantic contribution is maintained through Neighbor-Guided Reconstruction, which rectifies the pruned tokens, allowing them to continue contributing in subsequent layers. In this way, the LLM ultimately receives a complete and semanti-

cally intact set of vision tokens.

3.1. Token Pruning in the Vision Encoder

Let l_p denote the index of the transformer block in the vision encoder where token pruning is applied. Given the input patch embeddings to block l_p , denoted as $\mathbf{H}_{l_p} \in \mathbb{R}^{L \times D}$, together with the embeddings from the preceding block \mathbf{H}_{l_p-1} , we compute a token-wise importance score s_i based on the simple *feature-difference* criterion:

$$s_i = \|\mathbf{h}_{i, l_p} - \mathbf{h}_{i, (l_p-1)}\|_2, \quad i = 1, \dots, L. \quad (1)$$

Let $\mathcal{I}_{\text{keep}}$ be the indices of the top- K tokens with the largest s_i , and \mathcal{I}_{rem} be the remaining indices. The retained and removed token embeddings at the pruning layer l_p are:

$$\mathbf{H}_{\text{keep}, l_p} = \mathbf{H}_{l_p}[\mathcal{I}_{\text{keep}}, :], \quad \mathbf{H}_{\text{rem}, l_p} = \mathbf{H}_{l_p}[\mathcal{I}_{\text{rem}}, :]. \quad (2)$$

3.2. Neighbor-Guided Reconstruction (NGR)

We visualize the behavior of pruned tokens and their nearest neighbors in Figure 2. Panel (a) shows that, in the unpruned model, the hidden state trajectory of a token expected to be pruned remains highly consistent with the mean trajectory of its top-10 most similar unpruned tokens. This consistency indicates that the evolution of pruned tokens can be well approximated by the updates of their similar neighbors. Panels (b) and (c) present the empirical distribution of L1 distances between pruned and kept tokens, demonstrating that the change of a pruned token is much closer to the mean change of its top-10 similar tokens than to that of randomly

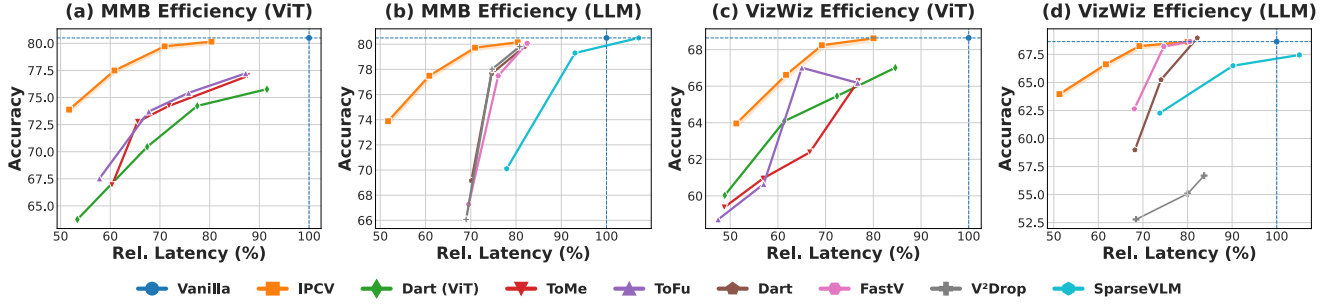


Figure 4. Efficiency comparison of IPCV vs. ViT/LLM baselines across datasets. (a) Accuracy vs. Rel. Latency for ViT baselines in MMB. (b) LLM baselines in MMB. (c) ViT baselines in VizWiz. (d) LLM baselines in VizWiz. **Rel. Latency** denotes total GPU inference time normalized to Vanilla. IPCV shows consistently strong efficiency-accuracy trade-offs on both datasets.

selected tokens. These findings support the design of our Neighbor-Guided Reconstruction mechanism.

NGR aims to reconstruct the removed tokens at a layer $l > l_p$ by transferring local updates from their nearest retained neighbors, thereby enabling pruned tokens to continue contributing contextual information either within current attention layer or subsequent processing stages.

Given the retained and removed index sets $\mathcal{I}_{\text{keep}}$ and \mathcal{I}_{rem} (and their embeddings $\mathbf{H}_{\text{keep}, l_p}$ and $\mathbf{H}_{\text{rem}, l_p}$), we can construct the rectified embeddings $\tilde{\mathbf{H}}_{\text{rem}, l}$ for any given layer $l > l_p$ in the vision transformer.

Neighbor selection. For each removed token $i \in \mathcal{I}_{\text{rem}}$ with feature \mathbf{h}_{i, l_p} , we find its k nearest neighbors among $\mathbf{H}_{\text{keep}, l_p}$ by minimizing the Euclidean distance:

$$\mathcal{N}_k(i) = \arg \min_{\mathcal{S} \subset \mathcal{I}_{\text{keep}}} \sum_{j \in \mathcal{S}} \|\mathbf{h}_{i, l_p} - \mathbf{h}_{j, l_p}\|_2. \quad (3)$$

Local update transfer. Let $\mathbf{H}_{\text{keep}, l}$ be the retained-token embeddings at the current layer l , and define the per-token update for the kept set from l_p to l as:

$$\Delta \mathbf{H}_{\text{keep}, l} = \mathbf{H}_{\text{keep}, l} - \mathbf{H}_{\text{keep}, l_p}. \quad (4)$$

We reconstruct each removed token i by adding the average updates of its k neighbors to its original embedding \mathbf{h}_{i, l_p} :

$$\tilde{\mathbf{h}}_{i, l} = \mathbf{h}_{i, l_p} + \frac{1}{k} \sum_{j \in \mathcal{N}_k(i)} \Delta \mathbf{h}_{j, l}. \quad (5)$$

Stacking all removed tokens yields $\tilde{\mathbf{H}}_{\text{rem}, l} \in \mathbb{R}^{|\mathcal{I}_{\text{rem}}| \times D}$. The complete NGR procedure is presented in Algorithm 1.

3.3. Attention Stabilization (AS)

Pruning at l_p alters the attention distribution because the removed tokens no longer participate in query-key interactions. To mitigate this with minimal overhead, IPCV temporarily retains the pruned tokens as keys and values for a few layers after pruning. Thus, they contribute context in attention while skipping the costly FFN layers [55].

Algorithm 1 Neighbor-Guided Reconstruction (NGR)

```

1: Input:  $\mathcal{I}_{\text{keep}}, \mathcal{I}_{\text{rem}}, \mathbf{H}_{\text{keep}, l_p}, \mathbf{H}_{\text{rem}, l_p}, \mathbf{H}_{\text{keep}, l}, k$ 
2: Output:  $\tilde{\mathbf{H}}_{\text{rem}, l}$ 
3: for each  $i \in \mathcal{I}_{\text{rem}}$  do
4:   Find  $\mathcal{N}_k(i) \subset \mathcal{I}_{\text{keep}}$  of size  $k$  minimizing
     $\sum_{j \in \mathcal{N}_k(i)} \|\mathbf{h}_{i, l_p} - \mathbf{h}_{j, l_p}\|_2$ 
5: end for
6:  $\Delta \mathbf{H}_{\text{keep}, l} \leftarrow \mathbf{H}_{\text{keep}, l} - \mathbf{H}_{\text{keep}, l_p}$ 
7: for each  $i \in \mathcal{I}_{\text{rem}}$  do
8:    $\tilde{\mathbf{h}}_{i, l} \leftarrow \mathbf{h}_{i, l_p} + \frac{1}{k} \sum_{j \in \mathcal{N}_k(i)} \Delta \mathbf{h}_{j, l}$ 
9: end for
10: Stack all  $\tilde{\mathbf{h}}_{i, l}$  to form  $\tilde{\mathbf{H}}_{\text{rem}, l}$ 

```

Concretely, for layers $l \in [l_p, l_p + \Delta l_{\text{max}}]$, the removed tokens are temporarily rectified via:

$$\tilde{\mathbf{H}}_{\text{rem}, l} = \text{NGR}(\mathbf{H}_{\text{rem}, l_p}, \mathbf{H}_{\text{keep}, l_p}, \mathbf{H}_{\text{keep}, l}). \quad (6)$$

At $l = l_p$, this is equivalent to directly using $\mathbf{H}_{\text{rem}, l_p}$.

Then, we restore the full token sequence $\mathbf{H}_{\text{full}, l} \in \mathbb{R}^{L \times D}$ by placing both retained and reconstructed tokens back to their corresponding original positions:

$$\begin{aligned} \mathbf{H}_{\text{full}, l}[\mathcal{I}_{\text{keep}}, :] &= \mathbf{H}_{\text{keep}, l}, \\ \mathbf{H}_{\text{full}, l}[\mathcal{I}_{\text{rem}}, :] &= \tilde{\mathbf{H}}_{\text{rem}, l}. \end{aligned} \quad (7)$$

The full sequence is provided as input to the multi-head attention module for bidirectional token interactions:

$$\mathbf{H}'_{\text{full}, l} = \text{Attention}(\mathbf{H}_{\text{full}, l}, \mathbf{H}_{\text{full}, l}, \mathbf{H}_{\text{full}, l}), \quad (8)$$

after which only the updated retained tokens are kept and forwarded to the FFN:

$$\mathbf{H}'_{\text{keep}, l} = \mathbf{H}'_{\text{full}, l}[\mathcal{I}_{\text{keep}}, :]. \quad (9)$$

This strategy is motivated by Skip-Vision [55], which shows that in transformer-based MLLMs, the feed-forward network (FFN) dominates computation for visual tokens, while attention is relatively lightweight. By enabling pruned tokens to skip the FFN but still join attention, IPCV preserves semantic aggregation with negligible extra FLOPs.

Table 1. Comparison of methods on Qwen2-VL. **Avg. Acc.** denotes the average percentage of performance relative to Vanilla; **Rel. Latency** shows total GPU inference time normalized to Vanilla (100%), measured on MMBench-EN.

Methods	GQA	MMB	MMB-CN	MME	POPE	SEED	VQA ^{text}	VizWiz	OCRBench	Avg. Acc.↑	Rel. Latency↓
Vanilla	61.5	80.5	78.7	2319	89.0	76.6	82.1	68.6	80.3	100%	100%
<i>ViT retain 50% tokens / LLM retain 50% tokens</i>											
DART (ViT)	57.6	74.2	72.7	2111	84.3	68.9	63.8	65.5	47.1	87.3%	77.5%
ToMe	59.1	74.2	73.5	2009	88.0	73.1	61.2	62.4	39.3	86.3%	71.8%
ToFu	59.0	75.4	73.9	1931	88.3	73.4	60.5	67.0	76.9	92.1%	75.8%
IPCV	60.5	79.7	76.7	2253	88.3	74.4	79.6	68.2	76.3	97.8%	70.9%
<i>ViT retain 35% tokens / LLM retain 35% tokens</i>											
DART (ViT)	55.1	70.5	69.2	1966	81.3	64.1	59.1	64.1	41.2	82.4%	67.4%
ToMe	58.2	72.8	71.6	1844	87.5	71.6	55.4	61.0	30.2	82.4%	65.5%
ToFu	58.7	73.7	72.7	1838	87.8	71.6	56.3	60.6	31.2	82.9%	67.8%
IPCV	58.8	77.5	75.3	2203	87.5	72.7	76.5	66.6	70.8	94.9%	60.8%
<i>ViT retain 20% tokens / LLM retain 20% tokens</i>											
DART (ViT)	50.0	63.8	63.0	1706	75.4	56.2	52.9	60.0	29.1	73.4%	53.4%
ToMe	56.2	66.9	67.0	1733	85.3	68.0	49.2	59.4	18.5	76.5%	60.4%
ToFu	56.3	67.5	67.7	1703	85.9	68.0	49.5	58.7	16.7	76.3%	57.8%
IPCV	55.8	73.9	73.5	1818	85.3	65.5	61.2	64.0	23.7	81.4%	51.7%
<i>ViT retain 100% tokens / LLM retain 20% tokens</i>											
DART	55.3	77.7	69.7	2035	83.9	67.5	66.0	65.2	46.0	86.4%	74.6%
FastV	58.6	77.5	76.5	2266	86.8	70.9	78.8	68.2	57.5	93.7%	76.1%
V ² Drop	55.1	78.0	76.2	2265	88.3	71.8	56.2	55.1	13.3	82.1%	74.7%
SparseVLM	58.1	79.3	76.9	2277	86.7	71.4	73.6	66.5	50.3	92.1%	93.0%
<i>ViT retain 100% tokens / LLM retain 5% tokens</i>											
DART	49.1	69.2	54.2	1764	77.7	55.6	40.4	59.0	33.6	71.9%	70.1%
FastV	50.2	67.3	67.9	1872	76.1	60.8	57.9	62.6	34.4	78.0%	69.5%
V ² Drop	47.9	66.1	67.4	1989	82.2	59.4	51.5	52.8	16.9	73.5%	69.0%
SparseVLM	49.3	70.1	69.0	1876	75.0	60.4	43.7	62.3	21.0	74.3%	77.9%

3.4. Reintegration at the Final ViT Layer

After the final ViT block l_{final} , IPCV merges the updated retained tokens $\mathbf{H}_{\text{keep}, l_{\text{final}}+1} \in \mathbb{R}^{|\mathcal{I}_{\text{keep}}| \times D}$ (denoting the output of l_{final}) with the newly reconstructed removed tokens $\tilde{\mathbf{H}}_{\text{rem}, l_{\text{final}}+1} \in \mathbb{R}^{|\mathcal{I}_{\text{rem}}| \times D}$ to restore the complete sequence:

$$\begin{aligned} \mathbf{H}_{\text{full}, l_{\text{final}}+1}[\mathcal{I}_{\text{keep}}, :] &= \mathbf{H}_{\text{keep}, l_{\text{final}}+1}, \\ \mathbf{H}_{\text{full}, l_{\text{final}}+1}[\mathcal{I}_{\text{rem}}, :] &= \tilde{\mathbf{H}}_{\text{rem}, l_{\text{final}}+1}. \end{aligned} \quad (10)$$

The resulting $\mathbf{H}_{\text{full}, l_{\text{final}}+1} \in \mathbb{R}^{L \times D}$ matches the original sequence length L prior to pruning. This Reintegration step guarantees that the downstream LLM receives the same number and ordering of visual tokens as in the uncompressed setting, thereby preserving both interface compatibility and semantic integrity without introducing additional computational overhead in earlier layers.

3.5. Compatibility with LLM-side Pruning

A key property of IPCV is the strict preservation of the visual token sequence: after vision-side pruning and NGR-based reconstruction, the sequence of visual tokens passed to the LLM exactly matches the original uncompressed sequence

in both length and ordering. This consistency in sequence structure ensures *interface compatibility* with the multimodal fusion module as well as the LLM input layer, allowing IPCV to be seamlessly integrated into existing architectures without requiring any modifications.

Consequently, IPCV can be seamlessly combined with existing LLM-side token pruning or acceleration techniques that assume a complete token set. For instance, methods such as FastV [3] and DART [49] can be directly applied to the LLM input sequence to further reduce computation by pruning less informative tokens in the language model's self-attention layers. In practice, IPCV serves as a drop-in vision-side token compression module that complements language-side efficiency methods in an orthogonal manner.

4. Experiments

4.1. Experimental Setup

Models and Baselines. We evaluate IPCV primarily on Qwen2-VL-7B-Instruct [45], an instruction-tuned vision-language model, and additionally on InternVL3-38B [62] to verify generalization across architectures. Base-

Table 2. Comparison of methods on video benchmarks with Qwen2-VL. **Rel. Latency** shows total GPU inference time normalized to Vanilla (100%), measured on MVBench.

Methods	MVBench	EgoSchema	MLVU	VideoMME				Avg. Acc. \uparrow	Rel. Latency \downarrow
				Overall	Short	Medium	Long		
Vanilla	66.1	62.0	59.8	57.7	70.4	54.6	48.0	100%	100%
<i>ViT retain 50% tokens / LLM retain 50% tokens</i>									
DART (ViT)	57.8	55.2	53.6	49.7	57.2	48.2	43.8	87.6%	87.0%
ToMe	50.4	48.8	49.0	44.8	48.3	43.6	42.4	78.8%	70.5%
ToFu	50.5	48.5	48.9	44.6	49.0	43.4	41.4	78.5%	73.9%
IPCV	64.0	58.4	57.8	55.1	67.6	51.7	46.1	95.7%	65.9%
<i>ViT retain 100% tokens / LLM retain 20% tokens</i>									
DART	58.9	59.2	55.1	53.0	64.1	49.4	45.4	92.1%	67.9%
FastV	50.9	54.7	53.4	49.4	58.2	45.7	44.4	85.6%	73.3%
V ² Drop	62.1	58.6	55.5	53.5	63.7	51.0	45.9	93.4%	69.9%
SparseVLM	60.9	61.8	56.5	54.0	65.7	49.8	46.6	94.5%	135.9%

Table 3. Comparison of different methods on InternVL3-38B. **Rel. Latency** shows total GPU inference time normalized to Vanilla (100%), measured on MMBench-EN.

Methods	GQA	MMB	MMB-CN	MME	POPE	VQA ^{text}	VizWiz	OCRBench	Avg. Acc. \uparrow	Rel. Latency \downarrow
Vanilla	60.8	89.0	88.9	2467	90.6	83.8	69.3	86.0	100%	100%
<i>ViT retain 40% tokens / LLM retain 40% tokens</i>										
DART (ViT)	60.8	85.0	85.4	2198	88.7	59.7	67.2	50.0	88.1%	63.9%
ToMe	60.2	82.2	80.9	2092	89.6	52.2	67.4	31.3	82.7%	61.7%
ToFu	59.8	83.9	83.5	2074	90.1	52.7	67.7	31.5	83.4%	61.9%
IPCV+FastV	61.2	84.5	83.2	2364	88.3	70.3	67.9	47.6	89.9%	64.4%
<i>ViT retain 100% tokens / LLM retain 5% tokens</i>										
DART	51.7	71.1	70.5	1916	77.6	46.4	60.1	33.5	73.6%	71.5%
FastV	54.0	76.6	77.0	1977	82.7	55.1	65.9	30.1	78.6%	70.7%
V ² Drop	43.9	59.5	59.1	1697	67.3	17.1	53.4	9.7	57.1%	70.5%
SparseVLM	51.4	74.6	73.5	1916	79.3	52.2	62.5	27.5	75.1%	73.4%

lines include training-free vision-side token compression methods (ToMe [1], ToFu [16]) and LLM-side token pruning methods (FastV [3], V²Drop [2], SparseVLM [60], DART [49]). For a direct comparison, we also implement a vision-side variant of DART, denoted DART (ViT).

Evaluation Details. To enable fair comparison between ViT-stage and LLM-stage methods, we report results using the overall acceleration ratio as the evaluation metric. For ViT-stage pruning methods, we adopt symmetric settings where both the ViT encoder and LLM decoder retain 50%, 35%, or 20% of tokens. For LLM-stage pruning methods, we use asymmetric settings that retain 100% of ViT tokens while pruning LLM tokens to 20% or 5%. Benchmarks cover diverse image datasets (GQA [14], MMBench [31], MME [9], POPE [20], SEED [17], TextVQA [42], VizWiz [11], OCRBench[32]) and video datasets (MVBench [19], EgoSchema [35], MLVU [61],

VideoMME [10]). Additional details on implementation and datasets are provided in Appendices C and D.

4.2. Main Results

Tables 1 and 2 summarize the accuracy–latency trade-off of IPCV and baselines on Qwen2-VL-7B across diverse benchmarks. Here, **Avg. Acc.** is the average percentage of performance relative to the vanilla model. **Rel. Latency** is total inference time normalized to vanilla (100%), measured on MMBench-EN for image and MVBench for video. To highlight the speed–accuracy trade-off, latencies are color-coded by relative runtime: dark blue ($\geq 80\%$), blue-green ($70\text{--}80\%$), green ($60\text{--}70\%$), and light green ($50\text{--}60\%$).

On image understanding tasks, IPCV consistently achieves a superior balance between performance and efficiency. Under moderate acceleration (70.9% vanilla runtime), it preserves 97.8% of the vanilla performance, out-

performing all baselines with comparable or higher runtime. At a higher speedup of 60.8% runtime, IPCV still retains 94.9% Avg. Acc, exceeding the next-best method by at least 12 points. In contrast, ViT-stage pruning baselines are prone to removing visual tokens that are critical for grounding textual understanding, resulting in pronounced accuracy degradation. This issue is particularly evident on visual detail-sensitive tasks (OCRBench, VizWiz, TextVQA), where IPCV proves more stable. LLM-stage pruning methods generally maintain reasonable accuracy under modest acceleration, but their performance declines noticeably when aiming for higher speedups, indicating a limited ability to sustain accuracy at high compression ratios.

On video understanding tasks, IPCV attains 95.7% of vanilla performance with lower inference latency, outperforming all baselines in this setting. Preserving text-critical visual cues also appears to be important for sustaining temporal-spatial reasoning. Similar to the image setting, ViT-stage pruning baselines suffer clear accuracy drops, while LLM-stage pruning methods, though relatively stable, still lag behind our method. IPCV reliably preserves multimodal reasoning across image and video benchmarks.

4.3. Experiments on InternVL3

To further examine the generalization of IPCV beyond Qwen2-VL, we conduct additional experiments on InternVL3-38B (Table 3). **Rel. Latency** is still measured on MMBench-EN for consistency. In this setting, we pair IPCV with FastV as the LLM-side pruner to test its overall effectiveness. The results show that IPCV continues to deliver favorable performance-efficiency trade-offs under this larger architecture: compared with alternative baselines, IPCV achieves higher accuracy at similar or lower runtime.

5. Analysis

5.1. Inference Efficiency Analysis

We evaluate efficiency on MMBench-EN, measuring total GPU inference latency and prefilling latency, together with FLOPs and KV cache usage (Table 4). IPCV achieves a favorable balance of accuracy and efficiency: latency drops to 70.9%, 60.8%, and 51.7% of the vanilla baseline, while maintaining strong accuracy over competing methods.

As shown in Figure 4, ViT-stage pruning achieves larger latency reductions but suffers sharper accuracy degradation, whereas LLM-stage methods plateau around 69% runtime and fails to deliver additional speedup under higher pruning ratios. Prefilling latency decreases proportionally with total latency, and results on VizWiz confirm IPCV’s effectiveness across benchmarks. Compared with LLM-stage pruning, ViT-stage methods such as IPCV retain more LLM tokens and consequently incur larger KV caches, yet this overhead remains acceptable for practical deployment. Moreover,

Table 4. Inference efficiency comparison on MMBench-EN. Latency columns show absolute time with relative percentage (normalized to Vanilla=100%).

Methods	Latency↓ (min:sec)	Prefill Latency↓ (min:sec)	FLOPs↓ (TFLOPs)	KV Cache↓ (MB)	Accuracy↑ (MMB)
Vanilla	61:12 (100%)	51:18 (100%)	31.9	76.6	80.5
<i>ViT retain 65% tokens / LLM retain 65% tokens</i>					
DART (ViT)	56:01 (91.5%)	46:22 (90.4%)	20.5	51.5	75.8
ToMe	53:37 (87.6%)	41:33 (81.0%)	20.6	51.5	77.0
ToFu	53:24 (87.3%)	41:26 (80.8%)	20.6	51.5	77.2
IPCV	49:11 (80.4%)	40:51 (79.6%)	22.0	54.2	80.2
<i>ViT retain 50% tokens / LLM retain 50% tokens</i>					
DART (ViT)	47:26 (77.5%)	37:24 (72.9%)	16.0	40.8	74.2
ToMe	43:57 (71.8%)	34:20 (66.9%)	16.2	40.7	74.2
ToFu	46:22 (75.8%)	34:30 (67.3%)	16.2	40.7	75.4
IPCV	43:25 (70.9%)	33:46 (65.8%)	18.0	44.6	79.7
<i>ViT retain 35% tokens / LLM retain 35% tokens</i>					
DART (ViT)	41:16 (67.4%)	29:33 (57.6%)	11.6	30.0	70.5
ToMe	40:05 (65.5%)	27:56 (54.5%)	12.1	30.0	72.8
ToFu	41:28 (67.8%)	27:37 (53.8%)	12.1	30.0	73.7
IPCV	37:14 (60.8%)	28:08 (54.8%)	14.1	34.9	77.5
<i>ViT retain 20% tokens / LLM retain 20% tokens</i>					
DART (ViT)	32:40 (53.4%)	27:28 (53.5%)	7.5	19.3	63.8
ToMe	36:56 (60.4%)	27:28 (53.5%)	8.3	19.3	66.9
ToFu	35:23 (57.8%)	27:20 (53.3%)	8.3	19.3	67.5
IPCV	31:39 (51.7%)	26:42 (52.1%)	10.5	25.3	73.9
<i>ViT retain 100% tokens / LLM retain 35% tokens</i>					
DART	50:07 (81.9%)	40:34 (79.1%)	20.4	34.9	79.8
FastV	50:28 (82.5%)	37:47 (73.7%)	19.7	32.2	80.1
V ² Drop	49:27 (80.8%)	38:29 (75.0%)	21.7	39.4	79.8
SparseVLM	65:33 (107.1%)	48:23 (94.3%)	19.0	29.4	80.5
<i>ViT retain 100% tokens / LLM retain 20% tokens</i>					
DART	45:40 (74.6%)	38:34 (75.2%)	17.9	25.3	77.7
FastV	46:33 (76.1%)	33:45 (65.8%)	17.1	22.6	77.5
V ² Drop	45:43 (74.7%)	34:40 (67.6%)	18.6	27.9	78.0
SparseVLM	56:56 (93.0%)	41:08 (80.2%)	16.5	20.3	79.3
<i>ViT retain 100% tokens / LLM retain 5% tokens</i>					
DART	42:55 (70.1%)	30:10 (58.8%)	15.4	15.9	69.2
FastV	42:33 (69.5%)	31:30 (61.4%)	14.6	13.0	67.3
V ² Drop	42:13 (69.0%)	31:36 (61.6%)	15.5	16.4	66.1
SparseVLM	47:42 (77.9%)	35:29 (69.2%)	14.1	11.3	70.1

FLOPs alone do not reliably predict latency, methods with similar FLOPs can yield different GPU times.

5.2. Compatibility in LLM-stage

Table 5 examines the compatibility of IPCV with representative LLM-stage token pruning methods. We observe that IPCV combined with FastV, DART and SparseVLM achieves comparable accuracy, all maintaining over 93% of vanilla performance. IPCV+V²Drop, on the other hand, shows more noticeable fluctuations across benchmarks. As seen in the InternVL3-38B results, V²Drop’s performance can be less stable under different architectures. While SparseVLM preserves accuracy, it often incurs higher inference latency, limiting practical efficiency. Thus, in practice we primarily consider FastV and DART as suitable LLM-stage token pruning methods to pair with IPCV.

Table 5. Combination of IPCV with different LLM-stage pruning methods. **Avg. Acc.** denotes the average percentage of performance relative to Vanilla.

Methods	GQA	MMB	MMB-CN	MME	POPE	SEED	VQA ^{text}	VizWiz	OCRBench	Avg. Acc.↑
Vanilla	61.5	80.5	78.7	2319	89.0	76.6	82.1	68.6	80.3	100%
<i>ViT retain 35% tokens / LLM retain 35% tokens</i>										
IPCV+DART (default)	58.8	77.5	75.3	2203	87.5	72.7	76.5	66.6	70.8	94.9%
IPCV+FastV	58.0	76.9	75.5	2205	87.0	71.5	74.1	66.9	64.0	93.3%
IPCV+V ² Drop	50.1	70.3	69.1	2048	84.4	64.7	17.4	52.9	5.4	73.3%
IPCV+SparseVLM	57.8	77.7	76.3	2220	87.0	71.9	74.0	66.2	62.6	93.3%

Table 6. Ablation study of IPCV. **Rel. Latency** shows inference latency normalized to Vanilla (100%), measured on the MMBench-EN. **Reint.** denotes Reintegration module.

Methods	GQA	MMB	MMB-CN	MME	POPE	SEED	VQA ^{text}	VizWiz	OCRBench	Avg. Acc.↑	Rel. Latency↓
Vanilla	61.5	80.5	78.7	2319	89.0	76.6	82.1	68.6	80.3	100%	100%
<i>ViT retain 35% tokens / LLM retain 35% tokens</i>											
IPCV	58.8	77.5	75.3	2203	87.5	72.7	76.5	66.6	70.8	94.9%	60.8%
IPCV (w/o AS)	59.2	76.6	74.8	2210	86.9	72.3	74.4	66.4	69.0	94.1%	56.1%
IPCV (w/o Reint.)	58.7	76.0	75.4	2211	87.6	72.5	75.4	66.3	72.4	94.7%	63.1%
IPCV (w/o AS, Reint.)	58.6	76.0	74.5	2197	87.4	71.9	73.7	65.7	69.0	93.6%	60.2%

5.3. Ablation Study

Table 6 presents the ablation analysis of IPCV. Removing either the AS module or the Reintegration step slightly reduces accuracy, and omitting both causes a more noticeable drop. These mechanisms provide such benefits with only a marginal impact on runtime. The key reason is that pruned tokens are reused only in lightweight attention while skipping the more costly feed-forward layers. The results confirm that AS and Reintegration are indeed complementary, enhancing IPCV without sacrificing efficiency.

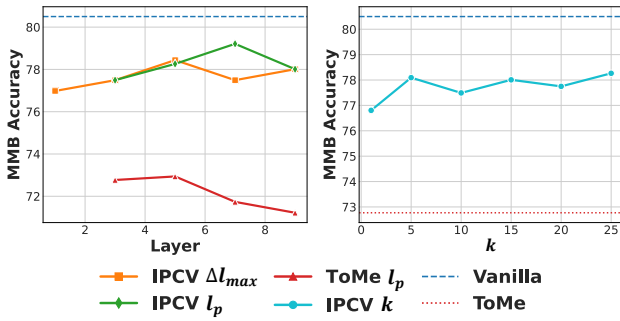


Figure 5. Sensitivity analysis of IPCV on MMBench-EN. **(Left)** Impact of pruning start layer l_p and AS depth Δl_{\max} . **(Right)** Impact of neighbor size k in NGR. ToMe is included as a reference.

5.4. Sensitivity Analysis

In our default configuration, the pruning start layer is $l_p = 3$, the Attention Stabilization depth is $\Delta l_{\max} = 7$, and the neighbor size in NGR is $k = 10$. We evaluate IPCV's sensitivity to these hyperparameters on MMBench-EN (see

Figure 5). Varying the Attention Stabilization depth Δl_{\max} shows that performance remains stable across a broad range (3–9). This indicates that a moderate depth suffices for stabilizing attention, with IPCV delivering consistent performance across choices of this parameter. For the pruning start layer l_p , later pruning is more accurate but less efficient, while earlier pruning is faster with a slight accuracy drop. We also analyze the sensitivity of the neighbor size k in NGR. A very small k can increase variance as reconstruction relies on too few neighbors, while a large k may introduce noise from less similar tokens. Empirically, IPCV remains stable over a wide range of k , confirming NGR's robustness.

6. Conclusion

We introduce IPCV, a training-free framework for token compression in MLLM visual encoders. IPCV combines early-stage pruning with two NGR-based modules: Attention Stabilization and Reintegration. This design enables aggressive token reduction in the ViT while preserving semantic information needed for downstream reasoning. Experiments on diverse image and video benchmarks demonstrate that IPCV achieves superior accuracy–efficiency trade-offs compared to existing training-free methods. IPCV also generalizes well across different model architectures. Looking ahead, IPCV provides a flexible foundation. Future work may focus on refining the reconstruction mechanism and further analyze the Attention Stabilization component to improve semantic preservation and computational efficiency, thereby enabling more powerful multimodal systems.

References

[1] Daniel Bolya, Cheng-Yang Fu, Xiaoliang Dai, Peizhao Zhang, Christoph Feichtenhofer, and Judy Hoffman. Token merging: Your vit but faster. In *Proceedings of the International Conference on Learning Representations (ICLR)*, 2023. 1, 2, 3, 6, 12

[2] Junjie Chen, Xuyang Liu, Zichen Wen, Yiyu Wang, Siteng Huang, and Honggang Chen. Variation-aware vision token dropping for faster large vision-language models. *arXiv preprint arXiv:2509.01552*, 2025. 6, 12

[3] Liang Chen, Haozhe Zhao, Tianyu Liu, Shuai Bai, Junyang Lin, Chang Zhou, and Baobao Chang. An image is worth 1/2 tokens after layer 2: Plug-and-play inference acceleration for large vision-language models. In *European Conference on Computer Vision*, pages 19–35. Springer, 2024. 2, 5, 6, 11

[4] Xuanyao Chen, Zhijian Liu, Haotian Tang, Li Yi, Hang Zhao, and Song Han. Sparsevit: Revisiting activation sparsity for efficient high-resolution vision transformer. In *Proceedings of the IEEE/CVF Conference on Computer Vision and Pattern Recognition (CVPR)*, pages 2061–2070, 2023. 3

[5] Zhaorun Chen, Yichao Du, et al. Mj-bench: Is your multi-modal reward model really a good judge for text-to-image generation? *arXiv preprint arXiv:2407.04842*, 2024. 1

[6] Long Cui, Weiyun Wang, Jie Shao, Zichen Wen, Gen Luo, Linfeng Zhang, Yanting Zhang, Yu Qiao, and Wenhui Wang. Vico: A training strategy towards semantic aware dynamic high-resolution. *arXiv preprint arXiv:2510.12793*, 2025. 1

[7] Alexey Dosovitskiy, Lucas Beyer, Alexander Kolesnikov, Dirk Weissenborn, Xiaohua Zhai, Thomas Unterthiner, Mostafa Dehghani, Matthias Minderer, Georg Heigold, Sylvain Gelly, Jakob Uszkoreit, and Neil Houlsby. An image is worth 16x16 words: Transformers for image recognition at scale. In *Proceedings of the International Conference on Learning Representations (ICLR)*, 2021. 2

[8] Danny Driess, Fei Xia, Mehdi S. M. Sajjadi, Corey Lynch, Aakanksha Chowdhery, Brian Ichter, Ayzaan Wahid, Jonathan Tompson, Quan Vuong, Tianhe Yu, Wenlong Huang, Yevgen Chebotar, Pierre Sermanet, Daniel Duckworth, Sergey Levine, Vincent Vanhoucke, Karol Hausman, Marc Toussaint, Klaus Greff, Andy Zeng, Igor Mordatch, and Pete Florence. Palm-e: An embodied multimodal language model. In *Proceedings of the 40th International Conference on Machine Learning*, pages 8469–8488. PMLR, 2023. 12

[9] Chaoyou Fu, Peixian Chen, Yunhang Shen, Yulei Qin, Mengdan Zhang, Xu Lin, Jinrui Yang, Xiawu Zheng, Ke Li, Xing Sun, Yunsheng Wu, Rongrong Ji, Caifeng Shan, and Ran He. Mme: A comprehensive evaluation benchmark for multimodal large language models. *arXiv preprint arXiv:2306.13394*, 2023. 6, 12

[10] Chaoyou Fu, Yuhai Dai, Yongdong Luo, Lei Li, Shuhuai Ren, Renrui Zhang, Zihan Wang, Chenyu Zhou, Yunhang Shen, Mengdan Zhang, Peixian Chen, Yanwei Li, Shaohui Lin, Sirui Zhao, Ke Li, Tong Xu, Xiawu Zheng, Enhong Chen, Caifeng Shan, Ran He, and Xing Sun. Video-mme: The first-ever comprehensive evaluation benchmark of multi-modal llms in video analysis. In *Proceedings of the IEEE/CVF Conference on Computer Vision and Pattern Recognition (CVPR)*, pages 24108–24118, 2025. 6, 13

[11] Danna Gurari, Qing Li, Abigale J. Stangl, Anhong Guo, Chi Lin, Kristen Grauman, Jiebo Luo, and Jeffrey P. Bigham. Vizwiz grand challenge: Answering visual questions from blind people. In *Proceedings of the IEEE Conference on Computer Vision and Pattern Recognition (CVPR)*, pages 3608–3617, 2018. 6, 12

[12] Yuhang Han, Xuyang Liu, Zihan Zhang, Pengxiang Ding, Junjie Chen, Donglin Wang, Honggang Chen, Qingsen Yan, and Siteng Huang. Filter, correlate, compress: Training-free token reduction for mllm acceleration. *arXiv preprint arXiv:2411.17686*, 2024. 2

[13] Peize He, Zichen Wen, Yubo Wang, Yuxuan Wang, Xiaoqian Liu, Jiajie Huang, Zehui Lei, Zhuangcheng Gu, Xiangqi Jin, Jiabing Yang, et al. Audiomarathon: A comprehensive benchmark for long-context audio understanding and efficiency in audio llms. *arXiv preprint arXiv:2510.07293*, 2025. 2

[14] Drew A Hudson and Christopher D Manning. Gqa: A new dataset for real-world visual reasoning and compositional question answering. In *Proceedings of the IEEE/CVF Conference on Computer Vision and Pattern Recognition (CVPR)*, pages 6700–6709, 2019. 6, 12

[15] Hengrui Kang, Siwei Wen, et al. Legion: Learning to ground and explain for synthetic image detection. *arXiv preprint arXiv:2503.15264*, 2025. 1

[16] Minchul Kim, Shangqian Gao, Yen-Chang Hsu, Yilin Shen, and Hongxia Jin. Token fusion: Bridging the gap between token pruning and token merging. In *Proceedings of the IEEE/CVF Winter Conference on Applications of Computer Vision*, pages 1383–1392, 2024. 1, 6, 12

[17] Bohao Li, Yuying Ge, Yixiao Ge, Guangzhi Wang, Rui Wang, Ruimao Zhang, and Ying Shan. Seed-bench: Benchmarking multimodal large language models. In *Proceedings of the IEEE/CVF Conference on Computer Vision and Pattern Recognition (CVPR)*, pages 13299–13308, 2024. 6, 12

[18] Junnan Li, Dongxu Li, Silvio Savarese, and Steven C. H. Hoi. Blip-2: Bootstrapping language-image pre-training with frozen image encoders and large language models. In *Proceedings of the International Conference on Machine Learning (ICML)*, 2023. 2

[19] Kunchang Li, Yali Wang, Yinan He, Yizhuo Li, Yi Wang, Yi Liu, Zun Wang, Jilan Xu, Guo Chen, Ping Luo, Limin Wang, and Yu Qiao. Mvbench: A comprehensive multimodal video understanding benchmark. In *Proceedings of the IEEE/CVF Conference on Computer Vision and Pattern Recognition (CVPR)*, pages 22195–22206, 2024. 6, 12

[20] Yifan Li, Yifan Du, Kun Zhou, Jinpeng Wang, Wayne Xin Zhao, and Ji-Rong Wen. Evaluating object hallucination in large vision-language models. *arXiv preprint arXiv:2305.10355*, 2023. 6, 12

[21] Yanwei Li, Chengyao Wang, and Jiaya Jia. Llama-vid: An image is worth 2 tokens in large language models. In *European Conference on Computer Vision*, pages 323–340. Springer, 2024. 3

[22] Youwei Liang, Chongjian Ge, Zhan Tong, Yibing Song, Jue Wang, and Pengtao Xie. Not all patches are what you need:

Expediting vision transformers via token reorganizations. *arXiv preprint arXiv:2202.07800*, 2022. 3

[23] Chenfei Liao, Wensong Wang, Zichen Wen, Xu Zheng, Yiyu Wang, Haocong He, Yuanhuiyi Lyu, Lutao Jiang, Xin Zou, Yuqian Fu, et al. Are we using the right benchmark: An evaluation framework for visual token compression methods. *arXiv preprint arXiv:2510.07143*, 2025. 2

[24] Bin Lin, Yang Ye, Bin Zhu, Jiaxi Cui, Munan Ning, Peng Jin, and Li Yuan. Video-llava: Learning united visual representation by alignment before projection. In *Proceedings of the 2024 Conference on Empirical Methods in Natural Language Processing*, pages 5971–5984, Miami, Florida, USA, 2024. Association for Computational Linguistics. 12

[25] Haotian Liu, Chunyuan Li, Qingyang Wu, and Yong Jae Lee. Visual instruction tuning. *arXiv preprint arXiv:2304.08485*, 2023. 1, 12

[26] Ting Liu, Liangtao Shi, Richang Hong, Yue Hu, Quanjun Yin, and Linfeng Zhang. Multi-stage vision token dropping: Towards efficient multimodal large language model. *arXiv preprint arXiv:2411.10803*, 2024. 1

[27] Xuyang Liu, Xiyan Gui, Yuchao Zhang, and Linfeng Zhang. Mixing importance with diversity: Joint optimization for kv cache compression in large vision-language models. *arXiv preprint arXiv:2510.20707*, 2025. 1

[28] Xuyang Liu, Yiyu Wang, Junpeng Ma, and Linfeng Zhang. Video compression commander: Plug-and-play inference acceleration for video large language models. *arXiv preprint arXiv:2505.14454*, 2025. 2

[29] Xuyang Liu, Ziming Wang, Yuhang Han, Yingyao Wang, Jiale Yuan, Jun Song, Bo Zheng, Linfeng Zhang, Siteng Huang, and Honggang Chen. Global compression commander: Plug-and-play inference acceleration for high-resolution large vision-language models. *arXiv preprint arXiv:2501.05179*, 2025. 1

[30] Xuyang Liu, Zichen Wen, Shaobo Wang, Junjie Chen, Zhishan Tao, Yubo Wang, Xiangqi Jin, Chang Zou, Yiyu Wang, Chenfei Liao, et al. Shifting ai efficiency from model-centric to data-centric compression. *arXiv preprint arXiv:2505.19147*, 2025. 1

[31] Yuan Liu, Haodong Duan, Yuanhan Zhang, Bo Li, Songyang Zhang, Wangbo Zhao, Yike Yuan, Jiaqi Wang, Conghui He, Ziwei Liu, Kai Chen, and Dahu Lin. Mmbench: Is your multi-modal model an all-around player? In *Proceedings of the European Conference on Computer Vision (ECCV)*, pages 216–233. Springer, 2024. 6, 12

[32] Yuliang Liu, Zhang Li, Mingxin Huang, Biao Yang, Wenwen Yu, Chunyuan Li, Xu-Cheng Yin, Cheng-Lin Liu, Lianwen Jin, and Xiang Bai. Ocrbench: on the hidden mystery of ocr in large multimodal models. *Science China Information Sciences*, 67(12):220102, 2024. 6, 12

[33] Ze Liu, Yutong Lin, Yue Cao, Han Hu, Yixuan Wei, Zheng Zhang, Stephen Lin, and Baining Guo. Swin transformer: Hierarchical vision transformer using shifted windows. In *Proceedings of the IEEE/CVF International Conference on Computer Vision (ICCV)*, pages 10012–10022, 2021. 3

[34] Junpeng Ma, Qizhe Zhang, Ming Lu, Zhibin Wang, Qiang Zhou, Jun Song, and Shanghang Zhang. Mmg-vid: Maximizing marginal gains at segment-level and token-level for efficient video llms. *arXiv preprint arXiv:2508.21044*, 2025. 2

[35] Karttikeya Mangalam, Raiymbek Akshulakov, and Jitendra Malik. Egoschema: A diagnostic benchmark for very long-form video language understanding. *Advances in Neural Information Processing Systems*, 36:46212–46244, 2023. 6, 12

[36] David Marr. *Vision: A computational investigation into the human representation and processing of visual information*. MIT press, 2010. 1

[37] Hyeonseob Nam, Jung-Woo Ha, and Jeonghee Kim. Dual attention networks for multimodal reasoning and matching. In *Proceedings of the IEEE Conference on Computer Vision and Pattern Recognition (CVPR)*, pages 299–307, 2016. 2

[38] Alec Radford, Jong Wook Kim, Chris Hallacy, Aditya Ramesh, Gabriel Goh, Sandhini Agarwal, Girish Sastry, Amanda Askell, Pamela Mishkin, Jack Clark, Gretchen Krueger, and Ilya Sutskever. Learning transferable visual models from natural language supervision. In *Proceedings of the 38th International Conference on Machine Learning (ICML)*, 2021. 12

[39] Alec Radford, Jong Wook Kim, Chris Hallacy, Aditya Ramesh, Gabriel Goh, Sandhini Agarwal, Girish Sastry, Amanda Askell, Pamela Mishkin, Jack Clark, Gretchen Krueger, and Ilya Sutskever. Learning transferable visual models from natural language supervision. In *Proceedings of the 38th International Conference on Machine Learning*, pages 8748–8763. PMLR, 2021. 1

[40] Yongming Rao, Wenliang Zhao, Benlin Liu, Jiwen Lu, Jie Zhou, and Cho-Jui Hsieh. Dynamicvitr: Efficient vision transformers with dynamic token sparsification. In *Advances in Neural Information Processing Systems (NeurIPS)*, 2021. 3

[41] Yuxin Shao, Zhen Li, Yifan Zhang, Xinyu Wang, and Hongsheng Li. Local-global attention: An adaptive mechanism for multi-scale feature integration. *arXiv preprint arXiv:2411.09604*, 2024. 2

[42] Amanpreet Singh, Vivek Natarajan, Meet Shah, Yu Jiang, Xinlei Chen, Dhruv Batra, Devi Parikh, and Marcus Rohrbach. Towards vqa models that can read. In *Proceedings of the IEEE/CVF Conference on Computer Vision and Pattern Recognition (CVPR)*, pages 8317–8326, 2019. 6, 12

[43] Yizheng Sun, Yanze Xin, Hao Li, Jingyuan Sun, Chenghua Lin, and Riza Batista-Navarro. Lvpruning: An effective yet simple language-guided vision token pruning approach for multi-modal large language models. In *Findings of the Association for Computational Linguistics: NAACL 2025*. Association for Computational Linguistics, 2025. 2

[44] Ashish Vaswani, Noam Shazeer, Niki Parmar, Jakob Uszkoreit, Llion Jones, Aidan N Gomez, Łukasz Kaiser, and Illia Polosukhin. Attention is all you need. *arXiv:1706.03762*, 2017. 1

[45] Peng Wang, Shuai Bai, Sinan Tan, Shijie Wang, Zhihao Fan, Jinze Bai, Keqin Chen, Xuejing Liu, Jialin Wang, Wenbin Ge, Yang Fan, Kai Dang, Mengfei Du, Xuancheng Ren, Rui Men, Dayiheng Liu, Chang Zhou, Jingren Zhou, and Junyang Lin. Qwen2-vl: Enhancing vision-language model's perception of the world at any resolution. *arXiv preprint arXiv:2409.12191*, 2024. 1, 5, 12

[46] Yiqi Wang, Wentao Chen, Xiaotian Han, Xudong Lin, Haiteng Zhao, Yongfei Liu, Bohan Zhai, Jianbo Yuan, Quanzeng You, and Hongxia Yang. Exploring the reasoning abilities of multimodal large language models (mllms): A comprehensive survey on emerging trends in multimodal reasoning. *arXiv preprint arXiv:2401.06805*, 2024. 1

[47] Yi Wang, Kunchang Li, Xinhao Li, Jiashuo Yu, Yinan He, Chenting Wang, Guo Chen, Baoqi Pei, Ziang Yan, Rongkun Zheng, Jilan Xu, Zun Wang, Yansong Shi, Tianxiang Jiang, Songze Li, Hongjie Zhang, Yifei Huang, Yu Qiao, Yali Wang, and Limin Wang. Internvideo2: Scaling foundation models for multimodal video understanding. *arXiv preprint arXiv:2403.15377*, 2024. 1

[48] Zichen Wen, Yifeng Gao, Weijia Li, Conghui He, and Linfeng Zhang. Token pruning in multimodal large language models: Are we solving the right problem? *arXiv preprint arXiv:2502.11501*, 2025. 2

[49] Zichen Wen, Yifeng Gao, Shaobo Wang, Junyuan Zhang, Qintong Zhang, Weijia Li, Conghui He, and Linfeng Zhang. Stop looking for important tokens in multimodal language models: Duplication matters more. *arXiv preprint arXiv:2502.11494*, 2025. 2, 5, 6, 12

[50] Zichen Wen, Shaobo Wang, Yufa Zhou, Junyuan Zhang, Qintong Zhang, Yifeng Gao, Zhaorun Chen, Bin Wang, Weijia Li, Conghui He, and Linfeng Zhang. Efficient multi-modal large language models via progressive consistency distillation. *arXiv preprint arXiv:2510.00515*, 2025. 1

[51] Zichen Wen, Yiyu Wang, Chenfei Liao, Boxue Yang, Junxian Li, Weifeng Liu, Haocong He, Bolong Feng, Xuyang Liu, Yuanhuiyi Lyu, et al. Ai for service: Proactive assistance with ai glasses. *arXiv preprint arXiv:2510.14359*, 2025. 1

[52] Minhao Xiong, Zichen Wen, Zhuangcheng Gu, Xuyang Liu, Rui Zhang, Hengrui Kang, Jiabing Yang, Junyuan Zhang, Weijia Li, Conghui He, Yafei Wang, and Linfeng Zhang. Prune2drive: A plug-and-play framework for accelerating vision-language models in autonomous driving. *arXiv preprint arXiv:2508.13305*, 2025. 2

[53] Yantai Yang, Yuhao Wang, Zichen Wen, Luo Zhongwei, Chang Zou, Zhipeng Zhang, Chuan Wen, and Linfeng Zhang. Efficientvla: Training-free acceleration and compression for vision-language-action models. *arXiv preprint arXiv:2506.10100*, 2025. 2

[54] Linli Yao, Lei Li, Shuhuai Ren, Lean Wang, Yuanxin Liu, Xu Sun, and Lu Hou. Deco: Decoupling token compression from semantic abstraction in multimodal large language models. *arXiv preprint arXiv:2405.20985*, 2024. 2

[55] Weili Zeng, Ziyuan Huang, Kaixiang Ji, and Yichao Yan. Skip-vision: Efficient and scalable acceleration of vision-language models via adaptive token skipping. In *Proceedings of the IEEE/CVF International Conference on Computer Vision (ICCV)*. IEEE, 2025. 2, 4

[56] Xiaohua Zhai, Basil Mustafa, Alexander Kolesnikov, and Lucas Beyer. Sigmoid loss for language image pre-training. In *Proceedings of the IEEE/CVF International Conference on Computer Vision (ICCV)*, pages 11975–11986, 2023. 1, 12

[57] Junyuan Zhang, Bin Wang, Qintong Zhang, Fan Wu, Zichen Wen, Jialin Lu, Junjie Shan, Ziqi Zhao, Shuya Yang, Ziling Wang, et al. Trivia: Self-supervised fine-tuning of vision-language models for table recognition. *arXiv preprint arXiv:2512.01248*, 2025. 1

[58] Junyuan Zhang, Qintong Zhang, Bin Wang, Linke Ouyang, et al. Ocr hinders rag: Evaluating the cascading impact of ocr on retrieval-augmented generation. In *Proceedings of the IEEE/CVF International Conference on Computer Vision (ICCV)*, pages 17443–17453, 2025.

[59] Qintong Zhang, Junyuan Zhang, Zhifei Ren, Linke Ouyang, Zichen Wen, Junbo Niu, Yuan Qu, Bin Wang, Ka-Ho Chow, Conghui He, et al. Docr-inspector: Fine-grained and automated evaluation of document parsing with vlm. *arXiv preprint arXiv:2512.10619*, 2025. 1

[60] Yuan Zhang, Chun-Kai Fan, Junpeng Ma, Wenzhao Zheng, Tao Huang, Kuan Cheng, Denis Gudovskiy, Tomoyuki Okuno, Yohei Nakata, Kurt Keutzer, and Shanghang Zhang. Sparsevlm: Visual token sparsification for efficient vision-language model inference. *arXiv preprint arXiv:2410.04417*, 2024. 1, 2, 6, 11

[61] Junjie Zhou, Yan Shu, Bo Zhao, Boya Wu, Shitao Xiao, Xi Yang, Yongping Xiong, Bo Zhang, Tiejun Huang, and Zheng Liu. Mlvu: A comprehensive benchmark for multi-task long video understanding. *arXiv preprint arXiv:2406.04264*, 2024. 6, 12

[62] Jinguo Zhu, Weiyun Wang, Zhe Chen, Zhaoyang Liu, Shenglong Ye, Lixin Gu, Hao Tian, Yuchen Duan, Weijie Su, Jie Shao, Zhangwei Gao, Erfei Cui, Xuehui Wang, Yue Cao, Yangzhou Liu, Xingguang Wei, Hongjie Zhang, Haomin Wang, Weiyi Xu, Hao Li, Jiahao Wang, Nianchen Deng, Songze Li, Yinan He, Tan Jiang, Jiapeng Luo, Yi Wang, Conghui He, Botian Shi, Xingcheng Zhang, Wenqi Shao, Junjun He, Yingtong Xiong, Wenwen Qu, Peng Sun, Penglong Jiao, Han Lv, Lijun Wu, Kaipeng Zhang, Huipeng Deng, Jiaye Ge, Kai Chen, Limin Wang, Min Dou, Lewei Lu, Xizhou Zhu, Tong Lu, Dahua Lin, Yu Qiao, Jifeng Dai, and Wenhui Wang. Internvl3: Exploring advanced training and test-time recipes for open-source multimodal models. *arXiv preprint arXiv:2504.10479*, 2025. 5

A. Baseline Details

To fairly evaluate our proposed IPCV framework, we compare it against representative baselines from two perspectives: MLLM language-side pruning and ViT compression.

A.1. MLLM Compression Methods

These methods are developed for MLLM token compression. They prune less informative tokens within the language model, without performing compression at the ViT stage.

FastV. FastV [3] prunes vision tokens in large vision-language models based on their attention scores. Tokens with low scores are removed early to accelerate inference.

SparseVLM. SparseVLM [60] proposes a text-aware visual token sparsification framework for efficient vision-language model inference. It leverages text tokens as raters to assess the significance of visual tokens, pruning redundant ones with a recycling mechanism to minimize information loss.

V²Drop. V²Drop [2] introduces a variation-aware pruning strategy for large vision-language models. By measuring variation across layers, it adaptively discards uninformative tokens rather than relying on fixed importance scores.

DART. DART [49] leverages token similarity to identify and remove duplicated tokens. This approach does not rely on explicit attention scores, making it compatible with FlashAttention and avoiding large GPU memory overhead.

A.2. ViT Compression Methods

ViT approaches are initially designed for vision-only transformers, targeting tasks like image classification. When applied to MLLMs, they operate directly on the vision encoder, merging or pruning visual tokens before the LLM-stage.

ToMe. ToMe [1] accelerates vision transformers by merging similar tokens. Using a bipartite matching algorithm based on attention keys, it gradually combines redundant tokens across layers to shorten the sequence length.

ToFu. ToFu [16] combines token pruning and merging in a unified framework. It adaptively chooses between them according to each layer’s characteristics and employs MLERP merging to better preserve feature norms.

B. More Related Works

Multimodal Large Language Models. Multimodal large language models (MLLMs) extend LLMs beyond text to vision and other modalities, enabling VQA, captioning, and multimodal reasoning [8, 25]. They typically couple a ViT pretrained with CLIP or SigLIP [38, 56], or Qwen2-VL’s dynamic-resolution ViT [45], with a lightweight projector and an LLM. Higher-resolution images or longer temporal windows yield longer visual sequences: Qwen2-VL encodes a 308×196 image into 5,220 tokens in the ViT stage and 1,305 after merging [45]; LLaVA maps 336×336 to 576 tokens, rising to 2,304 at 672×672 [25]; Video-LLaVA (8 frames) produces 2,048 tokens [24]. The resulting abundance of tokens strains the vision encoder and cross-modal layers, increasing compute and latency.

C. Implementation

All experiments are conducted on Nvidia GPUs. Qwen2-VL-7B-Instruct is evaluated on image benchmarks using RTX 4090 (48GB), and on video benchmarks using A100-80G. InternVL3-38B is evaluated on image benchmarks using A100-80G. For ToMe and ToFu, we follow the original implementations with a minor modification: tokens are reduced proportionally across layers until the target sparsity is reached. Other baseline settings follow the original papers.

D. Datasets

Our evaluation spans a diverse set of benchmarks for both image and video understanding.

D.1. Image Datasets

GQA. GQA [14] is built upon images, scene graphs, and compositional questions. It provides detailed annotations of entities, attributes, and their relationships, together with diverse queries that require multi-step reasoning, spatial understanding, and logical inference.

MMBench. MMBench [31] comprises over 3,000 multiple-choice questions across 20 fine-grained ability dimensions such as object localization and social reasoning. Each dimension contains more than 125 questions.

MME. MME [9] contains 14 subtasks covering perception (e.g., object existence, count, OCR) and cognition (e.g., commonsense reasoning, calculation, translation). All instruction-answer pairs are manually constructed in concise yes/no format for straightforward evaluation.

POPE. POPE [20] provides a polling-based evaluation benchmark designed to measure object hallucination in large vision-language models. It reformulates hallucination detection as a binary yes/no probing task about the presence of specific objects in an image.

SEED. SEED [17] introduces a large-scale benchmark with human-annotated multiple-choice questions across 27 dimensions, providing hierarchical evaluation of MLLMs from image-text comprehension to joint text-image generation.

TextVQA. TextVQA [42] is built from natural images in Open Images containing textual elements, paired with human-posed questions requiring reading the embedded text. It is designed to test whether models can integrate OCR outputs with visual reasoning to answer text-centric questions.

VizWiz. VizWiz [11] is a goal-driven VQA dataset built from images taken and spoken questions asked by blind people using a mobile phone application. It is designed to evaluate models in realistic assistive scenarios, where images may be low quality, questions conversational, and some visual questions inherently unanswerable.

OCRBench. OCRBench [32] evaluates large multimodal models on five OCR-related tasks, including text recognition, text-centric and document VQA, key information extraction, and handwritten expression recognition, aiming to expose their limitations on text-heavy vision tasks.

D.2. Video Datasets

MVBench. MVBench [19] systematically converts static image tasks into dynamic, defining 20 temporal understanding tasks spanning perception to cognition. It provides multiple-choice QAs generated from 11 public video datasets.

EgoSchema. EgoSchema [35] is a benchmark of long egocentric video clips with multiple-choice questions, designed to test very long-form video-language understanding. It introduces temporal certificates to measure intrinsic temporal hardness and exposes limitations in long-term reasoning.

MLVU. MLVU [61] is built from diverse videos lasting minutes to hours across real and simulated domains. It defines

nine tasks, such as summarization, action counting, and ordering, to evaluate models on complex long-video reasoning. **Video-MME**. Video-MME [10] contains 900 videos from six domains (e.g., knowledge, film & television, and multi-lingual) with 2,700 multiple-choice questions. The videos range from 11 seconds to 1 hour with subtitles and audio.

E. Theoretical Analysis

This section provides a theoretical analysis of perturbations arising from ViT-stage pruning and Reintegration.

Assumption E.1 (Hausdorff-Lipschitz Continuity). We assume the ViT mapping F from layer l_p to the output of l_{final} is L_{ViT} -Lipschitz with respect to the Hausdorff distance. Formally, for any two sets $\mathcal{X}, \mathcal{Y} \subset \mathbb{R}^d$ and any indices $i \in \text{Idx}(\mathcal{X}), j \in \text{Idx}(\mathcal{Y})$, where $\text{Idx}(\cdot)$ denotes the token index set, we assume index correspondence is preserved across layers. Then we have

$$\|F_i(\mathcal{X}) - F_j(\mathcal{Y})\|_2 \leq L_{\text{ViT}} d_H(\mathcal{X}, \mathcal{Y}),$$

where $F_i(\cdot)$ denotes the final-layer output at position i . d_H denotes the Hausdorff distance under the Euclidean norm:

$$d_H(\mathcal{X}, \mathcal{Y}) := \max \left\{ \sup_{x \in \mathcal{X}} \inf_{y \in \mathcal{Y}} \|x - y\|_2, \sup_{y \in \mathcal{Y}} \inf_{x \in \mathcal{X}} \|x - y\|_2 \right\}.$$

Assumption E.2 (Bounded embeddings). There exists a constant $B > 0$ s.t. all token embeddings at layer l_p satisfy

$$\|\mathbf{h}_{i, l_p}\|_2 \leq B, \quad \forall i.$$

Lemma E.3 (Pointwise deviation bound). *Consider the full token set \mathcal{X} at layer l_p , with $\mathcal{Y} \subset \mathcal{X}$ denoting the subset retained after pruning. For any $i \in \text{Idx}(\mathcal{X})$ and $r \in \text{Idx}(\mathcal{Y})$, we define the token update by:*

$$\Delta_i := F_i(\mathcal{X}) - \mathbf{h}_{i, l_p}, \quad \Delta_r := F_r(\mathcal{Y}) - \mathbf{h}_{r, l_p},$$

Then the following bound holds:

$$\|\Delta_i - \Delta_r\|_2 \leq \|\mathbf{h}_{i, l_p} - \mathbf{h}_{r, l_p}\|_2 + L_{\text{ViT}} d_H(\mathcal{X}, \mathcal{Y}).$$

Proof. By Assumption E.1 we have, for any output token $F_i(\mathcal{X}) \in F(\mathcal{X})$ and $F_r(\mathcal{Y}) \in F(\mathcal{Y})$

$$\|F_i(\mathcal{X}) - F_r(\mathcal{Y})\|_2 \leq L_{\text{ViT}} d_H(\mathcal{X}, \mathcal{Y}).$$

Therefore the deviation of token updates is bounded by

$$\begin{aligned} \|\Delta_i - \Delta_r\|_2 &= \|F_i(\mathcal{X}) - F_r(\mathcal{Y}) - (\mathbf{h}_{i, l_p} - \mathbf{h}_{r, l_p})\|_2 \\ &\leq \|F_i(\mathcal{X}) - F_r(\mathcal{Y})\|_2 + \|\mathbf{h}_{i, l_p} - \mathbf{h}_{r, l_p}\|_2 \\ &\leq \|\mathbf{h}_{i, l_p} - \mathbf{h}_{r, l_p}\|_2 + L_{\text{ViT}} d_H(\mathcal{X}, \mathcal{Y}), \end{aligned}$$

which proves the stated pointwise bound. \square

Remark E.4. By Assumption E.2, both $\|\mathbf{h}_{i, l_p} - \mathbf{h}_{r, l_p}\|_2$ and $d_H(\mathcal{X}, \mathcal{Y})$ are at most $2B$. Substituting these bounds into the pointwise inequality gives

$$\|\Delta_i - \Delta_r\|_2 \leq 2B (L_{\text{ViT}} + 1).$$

Theorem E.5 (NGR Reconstruction Error). *For each removed token i , the NGR reconstruction satisfies the bound*

$$\|\tilde{\mathbf{h}}_{i, l_{\text{final}}+1} - \mathbf{h}_{i, l_{\text{final}}+1}\|_2 \leq 2B (L_{\text{ViT}} + 1).$$

Here $\tilde{\mathbf{h}}_{i, l_{\text{final}}+1}$ denotes the reconstructed hidden state of pruned token i via NGR, and $\mathbf{h}_{i, l_{\text{final}}+1}$ the true hidden state without pruning. Consequently, the Hausdorff distance between the uncompressed final-layer set \mathcal{X}' and the reconstructed set $\hat{\mathcal{X}'}$ is bounded by

$$d_H(\mathcal{X}', \hat{\mathcal{X}'}) \leq 2B (L_{\text{ViT}} + 1).$$

Sketch. Recall that

$$\tilde{\mathbf{h}}_{i, l_{\text{final}}+1} - \mathbf{h}_{i, l_{\text{final}}+1} = \frac{1}{k} \sum_{r \in \mathcal{N}_k(i)} (\Delta_r - \Delta_i),$$

By the triangle inequality,

$$\|\tilde{\mathbf{h}}_{i, l_{\text{final}}+1} - \mathbf{h}_{i, l_{\text{final}}+1}\|_2 \leq \frac{1}{k} \sum_{r \in \mathcal{N}_k(i)} \|\Delta_r - \Delta_i\|_2.$$

From the Remark E.4 we obtain the worst-case bound $\|\Delta_r - \Delta_i\|_2 \leq 2B (L_{\text{ViT}} + 1)$ for any r . Hence each term in the sum is bounded by $2B (L_{\text{ViT}} + 1)$, so the average yields the desired inequality. \square

F. Visual Examples of Token Compression

Figure 6 presents diverse image examples of IPCV compression in the ViT stage. Without text guidance, our method tends to remove less informative regions, alleviating the impact of pruning on fine-grained content.

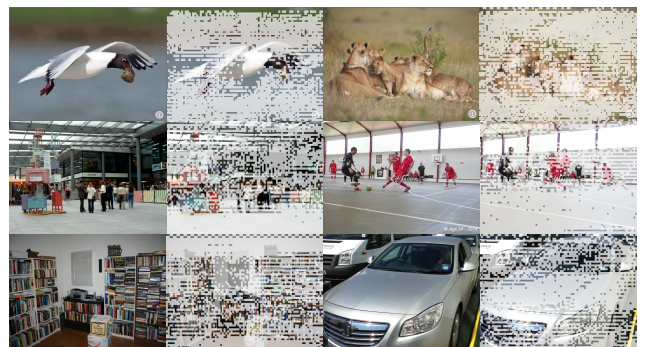


Figure 6. Original and compressed image pairs in the ViT-stage.